Simulation of dynamical quantum phase transition using variational quantum algorithms

Shintaro Ae*
Department of Applied Physics, The University of Tokyo, Tokyo 113-8656, Japan
(Dated: January 14, 2024)

Dynamics of the massive Schwinger model with a topological θ term is simulated using variational quantum algorithms to observe the dynamical quantum phase transition. Previous studies reported that the rate function exhibits kinks depending on the quench of θ parameter. Given an initial θ value, the ground state is calculated by the variational quantum eigensolver. After the quench, dynamics are simulated by variational quantum simulation. Although the kink itself is not observed due to the finite-volume effect, the overall dynamics of the rate function agrees with the exact diagonalization result. Moreover, it is reported that the performance of variational quantum simulation is improved using the condition number.

I. INTRODUCTION

Variational simulation using quantum computers has promising applications in many fields. One of the fields that quantum computers can play an active role is particle physics. A recent paper [13] confirmed a dynamical quantum phase transition of the $(1+1)$-dimensional quantum electrodynamics model (Schwinger model) and established the topological order parameter. In this study, dynamical phase transition of the Schwinger model is simulated using variational quantum algorithms. Although the IonQ quantum computer is once used to simulate the phase transition [8], its protocol can be only utilized when the topological theta term changes from 0 to π. In this study, the general simulation protocol for the quench of the Schwinger model and its results are presented.

Two quantum algorithms are used for the simulation: the Variational Quantum Eigensolver (VQE) and the Variational Quantum Simulation (VQS) [12]. VQE algorithms are utilized to determine the ground state and the ground energy of the system. VQE employs an ansatz with a few parameters. Parameters are adjusted so that the ansatz can represent various quantum states. VQS is used to evolve the quantum state after the quantum quench, which is the sudden change of topological θ parameter. A quench physically signifies a sudden change of the external field [9]. VQS also uses the same ansatz as the VQE. By changing the parameters of the ansatz, time evolution after the quench is simulated.

This paper is organized as follows: Section II briefly describes the dynamical quantum phase transition of the model. Section III describes the detailed simulation method. During simulation, it became clear that the use of the condition number stabilizes the VQS. Its method is explained on Appendix A. Simulation results are described in Section IV. Section V is for discussion and conclusion. Source code is publicized in the Appendix B.

* Student ID: 03-230526; aes93@g.ecc.u-tokyo.ac.jp

II. DYNAMICAL QUANTUM PHASE TRANSITION

The Lagrangian [5] of the Schwinger model with a topological theta term in the continuum is given by

$$\mathcal{L} = -\frac{1}{4}F_{\mu\nu}F^{\mu\nu} + \frac{g\theta}{4\pi}\epsilon_{\mu\nu}F^{\mu\nu} + i\bar{\psi}\gamma^{\mu}(\partial_{\mu} + igA_{\mu})\psi - m\bar{\psi}\psi, \tag{1}$$

where ψ is the fermion and m its mass, g the gauge coupling.

The second term on the right-hand side of the Lagrangian is called the topological theta term. Zache et al. [13] reported that after a sufficient change in θ, dynamical quantum phase transition occurs. Suppose $\theta(t) = \theta_0$ for $t < 0$, the entire system is stationary, and let $|\Omega\rangle$ denote that stationary ground eigenstate. At $t = 0$, θ changes abruptly and the whole system exhibits the dynamics. Let $\bar{U}(t)$ be the system's unitary operator, and the state at time $t = t(> 0)$ is given by $|\phi(t)\rangle = \bar{U}(t)\,|\Omega\rangle$. The reported dynamical phase transition can be observed with an intensive rate function, defined as follows.

$$\Gamma(t) := \lim_{N\to\infty}\left\{-\frac{1}{N}\log(|L(t)|)\right\} \tag{2}$$

N is the system size, and should be significantly large because finite-volume effect appears when N is small. $L(t)$ is called the Loschmidt echo, and is defined by

$$L(t) = \langle\Omega|\bar{U}(t)|\Omega\rangle\,. \tag{3}$$

One characteristic of the dynamical phase transition is non-analyticities in the rate function. By increasing the quench of θ at $t = 0$, a kink on the graph of rate function starts appearing. For small quenches $|\Delta\theta| < \pi/2$, the graph is entirely analytic. For large quenches $|\Delta\theta| > \pi/2$, the rate function exhibits non-analytic kinks. These kinks are more apparent for weaker coupling $g/m \to 0$ [13].

III. SIMULATION PROTOCOL

A. Simulation Overview

To calculate the Loschmidt echo in Eq. 3, a combination of VQE and VQS is used. First, we prepare the ground state $|\Omega\rangle$ by using VQE. Let λ be a set of parameters and $U(\lambda)$ be an ansatz in the quantum computer, which is obviously different from system's unitary operator $\bar{U}(t)$. Then VQE provides the initial parameter $\lambda(0)$ with $|\Omega\rangle \simeq U(\lambda(0))\,|0\rangle$. In this experiment, the initial state for the quantum computation is written as $|0\rangle$. Using VQS, the time evolution of the parameters $\lambda(t)$ is calculated with the same ansatz. With the calculated $\lambda(t)$, we obtain a unitary operator is $U(\lambda(t))$,

$$\bar{U}(t)\,|\Omega\rangle \simeq U(\lambda(t))\,|0\rangle\,. \tag{4}$$

Although the Loschmidt echo itself is difficult to measure, the absolute value of the Loschmidt echo $|L(t)|$ is measurable using the following method.

1. Apply the $U(\lambda(t))$ gate and $U^\dagger(0)$ gate to $|0\rangle$
2. Measure the probability of $|0\rangle$ of the state $U^\dagger(\lambda(0))U(\lambda(t))\,|0\rangle$. The probability equals $|L(t)|^2 \simeq |\,\langle 0|U^\dagger(\lambda(0))U(\lambda(t))|0\rangle\,|^2$.

All simulations are performed on the author's local environment using Qiskit. The source code available in Appendix B. A detailed simulation protocol is explained below.

B. System's Hamiltonian

To simulate time evolution, the Schwinger model with the Lagrangian in Eq. 1 in the continuum is discretized onto a lattice. After employing techniques such as Kogut and Susskind's method [2] for staggered fermions and Jordan-Wigner transformation, the Hamiltonian of the Schwinger model is obtained [5]:

$$\begin{aligned} H = J\sum_{n=0}^{N-2}\left[\sum_{i=0}^{n}\frac{Z_i+(-1)^i}{2}+\frac{\theta}{2\pi}\right]^2 \\ +\frac{w}{2}\sum_{n=0}^{N-2}[X_nX_{n+1}+Y_nY_{n+1}]+\frac{m}{2}\sum_{n=0}^{N-1}(-1)^nZ_n, \end{aligned} \tag{5}$$

where $J=\frac{ag^2}{2}, w=\frac{1}{2a}$,and $q=\frac{\theta}{2\pi}$. Expanding all the terms, the Hamiltonian is further transformed to

$$\begin{aligned} H = &\sum_{i=1}^{N-2}\sum_{j=0}^{i-1}\frac{J}{2}(N-1-i)Z_iZ_j \\ &+\sum_{i=0}^{N-1}\left[\frac{J}{2}\left\lfloor\frac{(N-i-(i \bmod 2))}{2}\right\rfloor\right. \\ &\qquad\left.+\frac{m}{2}(-1)^i+\frac{\theta J}{2\pi}(N-1-i)\right]Z_i \\ &+\sum_{i=0}^{N-2}\frac{w}{2}(X_iX_{i+1}+Y_iY_{i+1})+(\text{const.}), \end{aligned} \tag{6}$$

where $\lfloor\cdot\rfloor$ is the floor function.

C. Ansatz

The ansatz used in this study is called the Hamiltonian Variational Ansatz(HVA). It utilizes the Pauli operators in the system's Hamiltonian, namely $X_iX_{i+1}+Y_iY_{i+1}$, Z_iZ_{i+1}, and Z_n. The parameters $(\boldsymbol{\alpha},\boldsymbol{\beta},\boldsymbol{\gamma})$ represent the angles of rotation generated by these Pauli strings. The ansatz is written as follows:

$$\begin{aligned} U(\boldsymbol{\alpha},\boldsymbol{\beta},\boldsymbol{\gamma}) = &\prod_{n:\text{even}}X_n\prod_{n=1}^{\lfloor\frac{(N-1)}{2}\rfloor}\exp\left(-i\frac{\alpha_n}{2}(X_{2n-1}X_{2n}+Y_{2n-1}Y_{2n})\right)\prod_{m=0}^{\lfloor\frac{N}{2}\rfloor-1}\exp\left(-i\frac{\alpha_m}{2}(X_{2m}X_{2m+1}+Y_{2m}Y_{2m+1})\right) \\ &\times\prod_{n=1}^{\lfloor\frac{N-1}{2}\rfloor}\exp\left(-i\frac{\beta_n}{2}Z_{2n-1}Z_{2n}\right)\prod_{m=0}^{\lfloor\frac{N}{2}\rfloor-1}\exp\left(-i\frac{\beta_m}{2}Z_{2m}Z_{2m+1}\right)\prod_{n=0}^{N-1}\exp\left(-i\frac{\gamma_n}{2}Z_n\right) \end{aligned} \tag{7}$$

For brevity, let $\lambda(t)$ denote the parameter set, $(\boldsymbol{\alpha},\boldsymbol{\beta},\boldsymbol{\gamma})$, all depending on time. Figure 1 visualizes the ansatz used for the experiment. The ansatz circuit is divided into four parts. The second part of the ansatz rotates the quantum state along the $X_nX_{n+1}+Y_nY_{n+1}$ axis, with the rotation angle represented by the parameter α_n. The third part of the ansatz rotates the states along the Z_nZ_{n+1} axis by the angle β_n. The last part rotates the states along the Z_n axis by the angle γ_n.

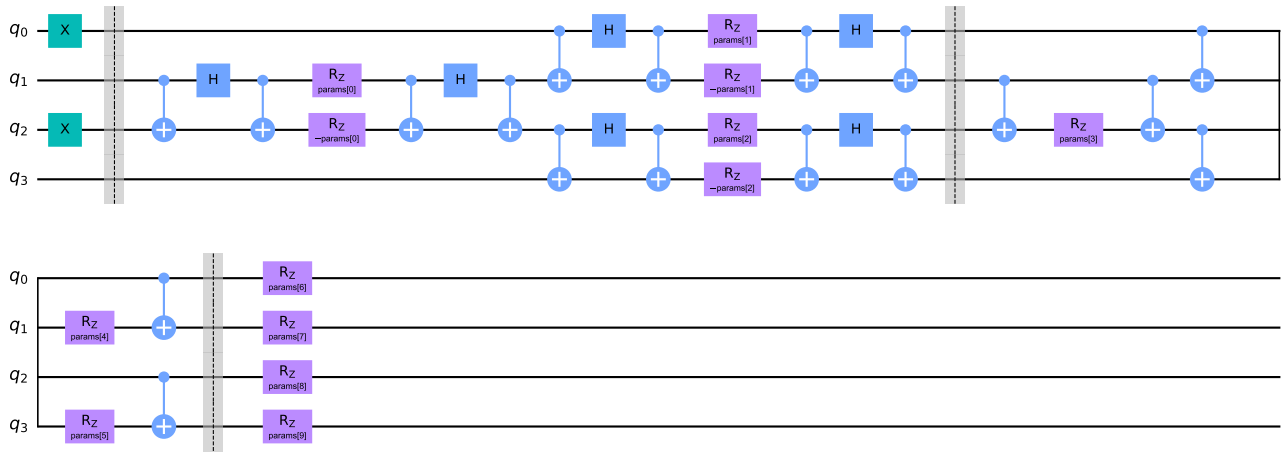

FIG. 1. Used ansatz for the simulation

D. Variational Quantum Eigensolver

VQE is used to estimate the lowest eigenvalue of the given Hamiltonian [10]. Given that E_0 is the lowest eigenvalue of the Hamiltonian H, the following inequality holds for all states $|\psi\rangle$:

$$\frac{\langle\psi| H |\psi\rangle}{\langle\psi|\psi\rangle} \geq E_0. \tag{8}$$

Thus, by adjusting the parameter λ of the ansatz, algorithm aims to minimize the expectation value of the Hamiltonian $\langle H\rangle = \langle 0| U^\dagger(\lambda) H U(\lambda) |0\rangle$, and the converged state is the ground state. Optimization method used in this simulation is the Constrained Optimization BY Linear Approximation (COBYLA) in the scipy package [1].

E. Variational Quantum Simulation

The VQS used for this experiment is based on McLachlan's variational principle [12]. As mentioned before, $|0\rangle$ denotes the initial state of the quantum computer. Let $|\phi\rangle$ denote the quantum state simulated by the ansatz,

$$|\phi(\lambda(t))\rangle := U(\lambda(t)) |0\rangle . \tag{9}$$

By projecting the Schrödinger equation onto the tangent subspace $\left\{\frac{\partial|\phi(\lambda)\rangle}{\partial\lambda_j}\right\}$, the following equations are obtained [12]:

$$\begin{aligned}
0 &= \left(\sum_i \frac{\partial \langle\phi(\lambda)|}{\partial\lambda_i}\delta\lambda_i\right)\left(\frac{d}{dt} + iH\right)|\phi(\lambda(t))\rangle \\
0 &= \left(\sum_i \frac{\partial \langle\phi(\lambda)|}{\partial\lambda_i}\delta\lambda_i\right)\left(\sum_j \frac{d\lambda_j}{dt}\frac{\partial|\phi(\lambda)\rangle}{\partial\lambda_j} + iH|\phi(\lambda(t))\rangle\right) \\
(^\forall i)\ &\sum_j \left(\frac{\partial \langle\phi(\lambda)|}{\partial\lambda_i}\frac{\partial|\phi(\lambda)\rangle}{\partial\lambda_j}\right)\frac{d\lambda_j}{dt} = -i\left(\frac{\partial \langle\phi(\lambda)|}{\partial\lambda_i} H|\phi(\lambda)\rangle\right)
\end{aligned} \tag{10}$$

Defining $A_{i,j}$ and C_i as follows, Eq. 10 becomes $\sum_j A_{i,j}\frac{d\lambda_j}{dt} = -iC_i$.

$$A_{i,j} = \frac{\partial \langle\phi(\lambda)|}{\partial\lambda_i}\frac{\partial|\phi(\lambda)\rangle}{\partial\lambda_j},\ C_i = \frac{\partial \langle\phi(\lambda)|}{\partial\lambda_i} H|\phi(\lambda)\rangle \tag{11}$$

Considering that only real parameters can be used, taking the real part of the equation is necessary. By taking the real part, the equation becomes

$$\sum_j A^R_{i,j}\frac{d\lambda_j}{dt} = C^I_i. \tag{12}$$

Furthermore, the global phase requires consideration. Suppose that the target state (state that should be reproduced by the ansatz, the theoretical quantum state in the Schwinger model) $|\psi(t)\rangle$ is represented by the trial state up to the global phase $\theta_0(t)$.

$$|\psi(t)\rangle \approx e^{i\theta_0(t)}|\phi(\lambda)\rangle \tag{13}$$

The Schrödinger equation gives

$$\sum_j \frac{\partial|\psi(t)\rangle}{\partial\lambda_j}\delta\lambda_j \approx -iH\delta t|\psi(t)\rangle , \tag{14}$$

and the substitution of $|\psi(t)\rangle$ with $e^{i\theta_0(t)}|\phi(\lambda(t))\rangle$ gives

$$\begin{aligned} &-i\delta t H e^{i\theta_0(t)}|\phi(\lambda)\rangle \\ =&e^{i\theta_0(t)}\sum_j \frac{\partial|\phi(\lambda)\rangle}{\partial\lambda_j}\delta\lambda_j m + i\,e^{i\theta_0(t)}\delta\theta_0|\phi(\lambda)\rangle \end{aligned} \tag{15}$$

By projecting Eq. 15 onto the tangent subspace $\left\{\frac{\partial|\phi(\lambda)\rangle}{\partial\lambda_j}\right\}$ again, the following equations are derived.

$$\begin{aligned} \sum_j M_{i,j}\frac{d\lambda_j}{dt} &= V_i, \\ M_{i,j} &= A^R_{i,j} + N_{i,j} \\ V_i = C_i + W_i &:= \sum_j (C_{i,j} + W_{i,j}) \end{aligned} \tag{16}$$

The summation of V_i is over each term of the Hamiltonian $H = \sum_j h_j\rho_j$, where ρ_j are the Pauli strings XX, YY, ZZ, and Z. $N_{i,j}$ and $W_{i,j}$ are the correction terms defined as follows:

$$\begin{aligned} N_{i,j} &= \frac{\partial\langle\phi(\lambda)|}{\partial\lambda_i}|\phi(\lambda)\rangle\frac{\partial\langle\phi(\lambda)|}{\partial\lambda_j}|\phi(\lambda)\rangle \\ W_{i,j} &= ih_j\frac{\partial\langle\phi(\lambda)|}{\partial\lambda_i}|\phi(\lambda)\rangle\langle\phi(\lambda)|\sigma_j|\phi(\lambda)\rangle\,. \end{aligned} \tag{17}$$

Eq. 16 implies that the evolution of the parameters λ can be calculated by measuring each element $A^R_{i,j}, N_{i,j}, C_{i,j}, W_{i,j}$. Measurement methods are explained in the following sections.

1. $A^R_{i,j}, C_i$

The estimation circuit for $A_{i,j}$ and C_i was originally proposed by Li and Benjamin [12]. $A_{i,j}$ and C_i are defined as

$$\begin{aligned} A_{i,j} &= \langle 0|\frac{\partial U^\dagger}{\partial\lambda_i}\frac{\partial U}{\partial\lambda_j}|0\rangle\,, \\ C_i &= \langle 0|\frac{\partial U^\dagger}{\partial\lambda_i}HU|0\rangle\,, \end{aligned} \tag{18}$$

where the ansatz U is given by $U = \prod_{n:\text{even}} X_n \times \prod_i \exp(i\frac{\lambda_j}{2}\sigma_i)$ with parameters λ_j and Pauli operators σ_j. Then, the partial differential of the ansatz with respect to each parameter is

$$\begin{aligned} \frac{\partial U}{\partial\lambda_j} &= \left(\prod_{n:\text{even}} X_n\right)\left(\frac{\partial}{\partial\lambda_j}e^{-i\frac{\lambda_N}{2}\sigma_N}\dots e^{-i\frac{\lambda_1}{2}\sigma_1}\right) \\ &= \left(\prod_{n:\text{even}} X_n\right)\Bigg[-\frac{i}{2}\left(e^{-i\frac{\lambda_N}{2}\sigma_N}\dots e^{-i\frac{\lambda_{j+1}}{2}\sigma_{j+1}}\right) \\ &\quad e^{-i\frac{\lambda_j}{2}\sigma_j}\sigma_j\left(e^{-i\frac{\lambda_{j-1}}{2}\sigma_{j-1}}\dots e^{-i\frac{\lambda_1}{2}\sigma_1}\right)\Bigg]. \end{aligned} \tag{19}$$

Although it may seem complicated, the method to measure Eq. 19 has already been discovered. Yuan's paper [12] describes the approach to measure

$$a\Re(e^{i\theta}\langle 0|V|0\rangle) \tag{20}$$

with

$$V = R_1^\dagger\dots R_{k-1}^\dagger U_k^\dagger R_k^\dagger\dots R_N^\dagger R_N\dots R_q U_q R_{q-1}\dots R_1 \tag{21}$$

using the circuit shown in Figure 2. This method can be employed to measure Eq. 19.

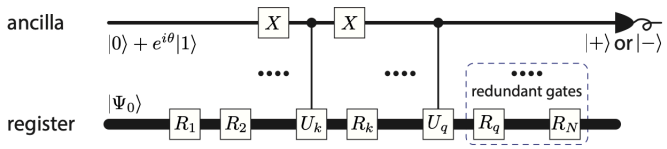

FIG. 2. Circuit to calculate Eq. 20. Figure cited from [12].

2. $N_{i,j}$

The correction term N_{ij} for the global phase is defined by

$$N_{i,j} = \frac{\partial\langle\phi(\lambda)|}{\partial\lambda_i}|\phi(\lambda)\rangle\frac{\partial\langle\phi(\lambda)|}{\partial\lambda_j}|\phi(\lambda)\rangle\,,$$

and can be expanded as follows:

$$\begin{aligned} N_{i,j} = &\frac{i}{2}\langle 0|\left(e^{i\frac{\lambda_1}{2}\sigma_1}\dots e^{i\frac{\lambda_{i-1}}{2}\sigma_{i-1}}\right)\sigma_i \\ &\left(e^{-i\frac{\lambda_{i-1}}{2}\sigma_{i-1}}\dots e^{-i\frac{\lambda_1}{2}\sigma_1}\right)|0\rangle \\ &\times\frac{i}{2}\langle 0|\left(e^{i\frac{\lambda_1}{2}\sigma_1}\dots e^{i\frac{\lambda_{j-1}}{2}\sigma_{j-1}}\right)\sigma_j \\ &\left(e^{-i\frac{\lambda_{j-1}}{2}\sigma_{j-1}}\dots e^{-i\frac{\lambda_1}{2}\sigma_1}\right)|0\rangle \\ =&-\frac{1}{4}\langle\sigma_i\rangle_{1\to i-1}\langle\sigma_j\rangle_{1\to j-1}\,, \end{aligned} \tag{22}$$

where $\langle\hat{A}\rangle_{1\to i}$ denotes taking the expectation value of the operator $\hat{A}$ for the state $e^{-i\frac{\lambda_i}{2}\sigma_i}\dots e^{-i\frac{\lambda_1}{2}\sigma_1}|0\rangle$.

3. $W_{i,j}$

The correction term W_i for the global phase is defined by

$$W_i = i\frac{\partial\langle\phi(\lambda)|}{\partial\lambda_i}|\phi(\lambda)\rangle\langle\phi(\lambda)|H|\phi(\lambda)\rangle\,. \tag{23}$$

Corresponding to each term of the Hamiltonian $H = \sum h_j\rho_j$, W_i is divided into $W_i = \sum_j W_{i,j}$. Each $W_{i,j}$

can be calculated as follows:

$$
\begin{aligned}
W_{ij} = -\frac{h_j}{2} \langle 0| \left(e^{i\frac{\lambda_1}{2}\sigma_1} \dots e^{i\frac{\lambda_{i-1}}{2}\sigma_{i-1}} \right) \sigma_i \\
\left(e^{-i\frac{\lambda_{i-1}}{2}\sigma_{i-1}} \dots e^{-i\frac{\lambda_1}{2}\sigma_1} \right) |0\rangle \\
\times \langle 0| \left(e^{i\frac{\lambda_1}{2}\sigma_1} \dots e^{i\frac{\lambda_N}{2}\sigma_N} \right) \rho_j \\
\left(e^{-i\frac{\lambda_N}{2}\sigma_N} \dots e^{-i\frac{\lambda_1}{2}\sigma_1} \right) |0\rangle \\
= -\frac{h_j}{2} \langle \sigma_i \rangle_{1\to i-1} \langle \rho_j \rangle_{1\to N} .
\end{aligned} \tag{24}
$$

IV. SIMULATION RESULTS

A. Variational Quantum Eigensolver

Figure 3 and 4 show the VQE results. Throughout the experiment, the parameters of the Hamiltonian (Eq. 6) are set to $J = 1$, $m = 1$, $w = 1$, and the number of qubits used for the simulation is 4. VQE iteratively updates the parameters of the ansatz (shown in Figure 1). For each iteration, expectation value of the Hamiltonian $\langle H \rangle$ is measured using shots or statevector. A shot is a statistical sampling of the Hamiltonian expectation value and the number of shots is varied: $10, 100, 1000, 10000, 100000$. The same 40 randomly selected initial states are used for each number of shots and the statevector simulation.

Figure 3 shows that the energy of the state approaches the exact minimum eigenvalue of the Hamiltonian. However, when the number of shots is not sufficient, several states get trapped in a local minimum state. A local minimum state appears to have the lowest cost function in the immediate vicinity. There seems to be a local minimum at $\langle E \rangle = -1$. When the number of shots is 1000, three optimizations converged to the local minimum. However, the number of optimizations that get trapped there seems to decrease. When the number of shot is 10000, the trapped optimizations are two, and when the number is 100000, only one optimization is trapped.

Figure 4 is the plot of fidelity between the exactly calculated ground state and the optimized state. Throughout this paper, fidelity between density matrix states ρ_1 and ρ_2 is defined as follows:

$$
F(\rho_1, \rho_2) = \left(\mathrm{Tr} \sqrt{\sqrt{\rho_1}\rho_2\sqrt{\rho_1}} \right)^2 . \tag{25}
$$

Fidelity is an indicator of closeness for quantum states [6]. When it is close to one, the two states are similar. Conversely, two states become orthogonal to each other when the fidelity reaches zero.

Figure 4 shows that the average of fidelity appraoches 1 as the number of shots increases, indicating that the exact ground state and the optimized state become more similar. The standard deviation decreases as the number of shots increases.

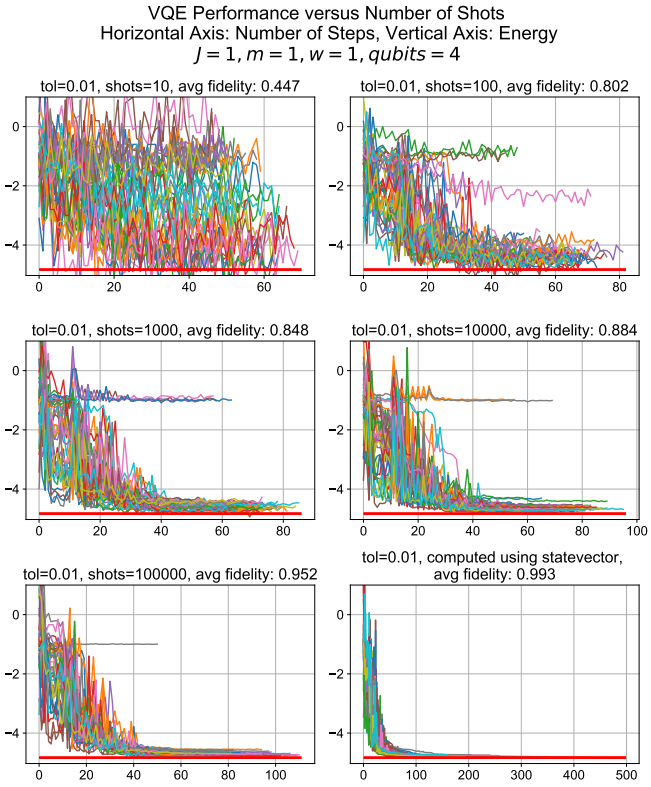

FIG. 3. VQE performance versus the number of shots. Repeated forty times from the same randomly selected forty initial states. The horizontal bold red line shows the minimum eigenvalue calculated by exact diagonalization. Fidelity is calculated between the exact ground state and optimized states. VQE method: COBYLA, max iteration: 500, tol (final accuracy in the optimization): 0.01.

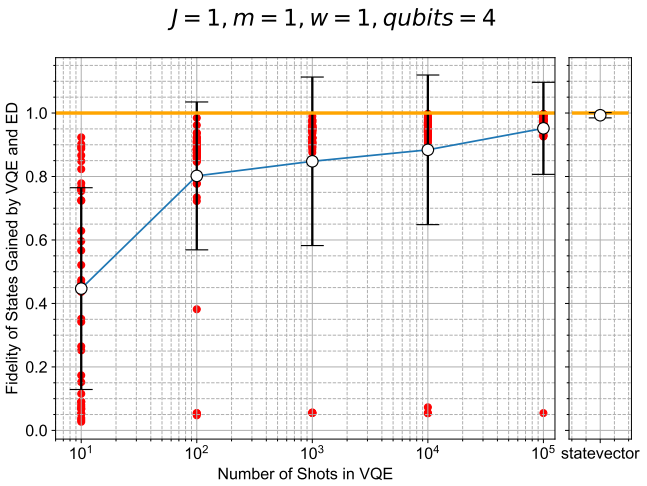

FIG. 4. Fidelity between the states obtained by VQE and exact diagonalization, changing the number of shots in VQE. 40 trials for each number of shots. Error bars show the standard deviation.

B. Variational Quantum Simulation

1. *VQS by statevector*

The evolution of the quantum state is first simulated using statevector simulation, where shot noise does not affect the results. Figure 5 shows the fidelity between the exact state and the VQS simulation. The number of steps is varied from 250 to 3000. All the simulations use the same initial parameters. Stability improves as the number of steps increases, although there is little apparent difference between 1000 steps and 3000 steps.

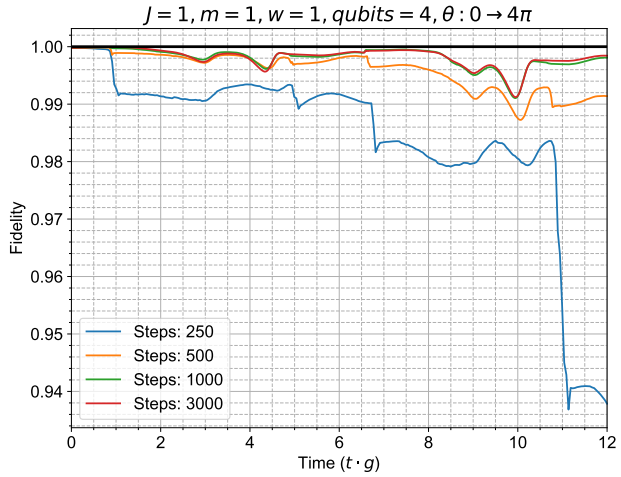

FIG. 5. Change of fidelity between quantum state calculated by exact diagonalization and state calculated by VQS with statevector simulation, depending on the number of steps for the time evolution.

2. *VQS by shots*

Concerning the VQS by shots, almost the same rate function performance was reproduced. However, when the number of shots decreases, a phenomenon we term *singularity* begins to appear. Figure 6 illustrates the fidelity between states calculated by VQS and exact diagnalization. It is evident that fidelity remains around 1 as the number of shot increases.

Of particular note is that the average of the shot number 1000/3162 is lower than the 25th percentile of 35/40 samples during the initial period of time evolution. This indicates that some fidelities drop rapidly to zero, causing the average to be lower than the 25th percentile. We found that this phenomenon is due to the statistical fluctuation of the $M_{i,j}$ in Eq. 16. When measuring the element of $M_{i,j}$, it is possible that $M_{i,j}$ approaches a singular matrix (matrix without an inverse). When it occurs, parameters λ are more sensitive to the noise of the measurement. To address this issue, we propose checking the

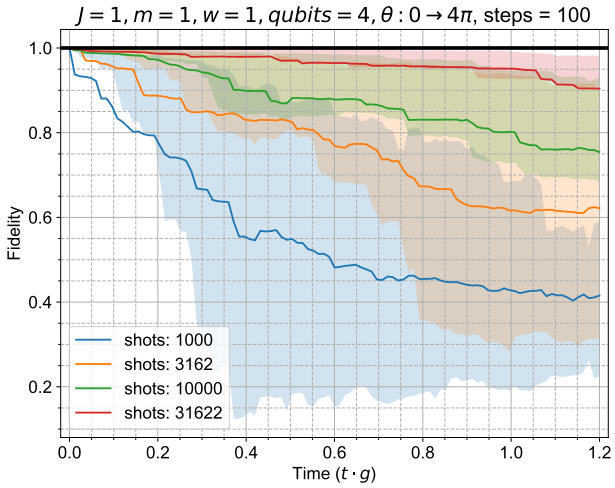

FIG. 6. Change of fidelity between the exact state calculated by exact diagonalization and the state calculated by VQS with shot noise, with the number of shots varied from 1000 (10^3) to 31622 ($10^{4.5}$). The same initial state is used for all simulations (fidelity: 0.999801). Solid curves represent the average, and error bands represent the 25-75 percentiles of 35 samples for shot numbers 1000, 10000, 31622, and 40 samples for shot number 3162.

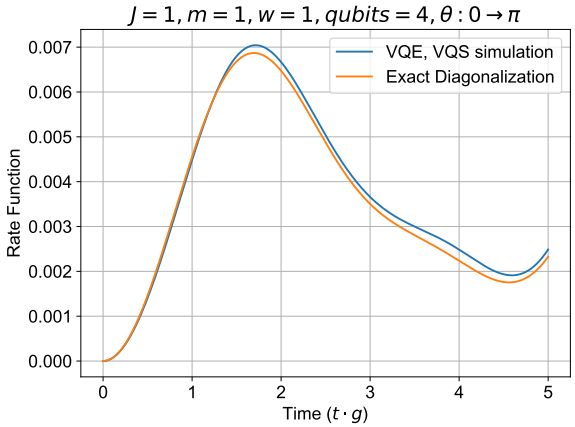

FIG. 7. Simulation of the rate function using exact diagonalization and VQE/VQS. Number of steps for VQS is 500.

condition number of the matrix during VQS. A detailed discussion is in Appendix A.

C. Rate Function

Figure 7 shows the dynamics of the rate function. Because the quench $\Delta\theta = \pi(> \pi/2)$ is strong enough, the graph should exhibit the kink. However, both the variational simulation and the exact diagonalization do not show the kink. The overall concave shape of the graph agrees with the previous study [13].

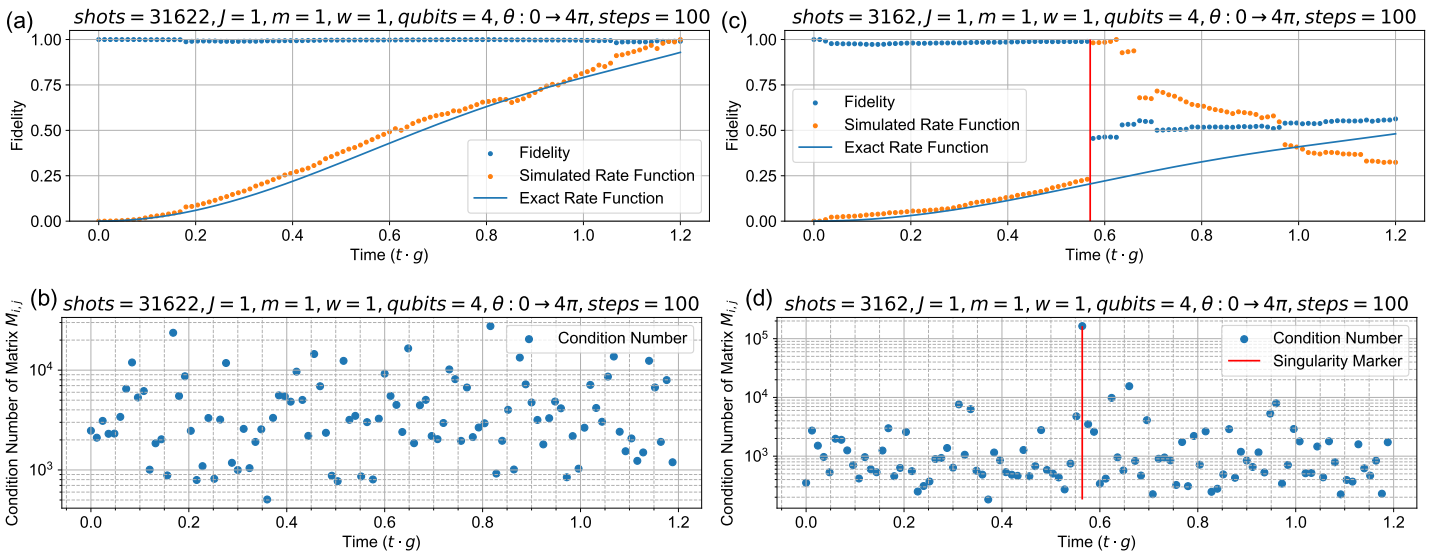

FIG. 8. Example of VQS with and without singularity. **(a)**: Rate function comparison between VQS simulation and exact diagonalization. Fidelity between the VQS results and the exact results is also plotted. The number of shots is 31622. **(b)**: Condition number of $M_{i,j}$ in the VQS simulation plotted in (a). **(c)**: Rate function comparison of VQS and exact diagonalization, and fidelity. The number of shots is 3162. **(d)**: Condition number of $M_{i,j}$ in the VQS simulation (c), red line shows the typical singularity observed in the VQS simulations with shots.

V. DISCUSSION AND CONCLUSION

In this study, the dynamics of the Schwinger model are explored using variational quantum algorithms, namely the Variational Quantum Eigensolver (VQE) and the Variational Quantum Simulation (VQS).

First, the VQE simulation results reveal both its merits and demerits. Figures 3 and 4 illustrate that most of the optimizations converge to the ground state, while it is noted that some optimizations converge to the local minima. Notably, the occurrence of such traps decreases with an increase of the number of shots in VQE. Further investigation into improving VQE, especially the reduction of the traps in local minima and scaling of the number of shots, is left for future study.

Second, VQS is employed for the dynamics simulation of the Schwinger model, based on McLachlan's variational principle. One of the benefit of integrating VQE and VQS is that VQS can reuse an existing VQE ansatz, and it is unnecessary to construct an entirely new ansatz. Figure 5 shows that the performance of VQS improves with an increase in the number of steps. Although VQS with the shot simulation faces the singularity problem, we demonstrate that calculating the condition number can effectively address this issue (see Appendix A).

Lastly, we were unable to observe the dynamical topological phase transition. It is expected that the rate function exhibits a non-analytic kink when the quench is strong enough ($\Delta\theta > \pi/2$). However, Figure 7 does not display kink, and the graph is entirely analytic. It is likely that finite-volume effects influenced the shape of the graph. These kinks are expected to appear in an infinite system size. However, the number of qubits in this simulation is four, implying only two Dirac fermions in our system. Previous study predicted that the critical time t_c of the phase transition corresponds to the top of the graph. While the concave analytic graph still exhibits the critical time t_c, calculation of the order parameter is needed to avoid the finite-volume effect [13].

ACKNOWLEDGMENTS

This work is part of the quantum computer summer camp at the International Center for Elementary Particle Physics (ICEPP) at The University of Tokyo. The author would like to thank Mr. Lento Nagano (ICEPP) for his great support and stimulating discussion. He would also like to express gratitude to Mr. Takayasu Matsuo and Mr. Shun Sato (Graduate School of Information Science and Technology, The University of Tokyo) for the discussion about the condition number algorithm.

Appendix A: VQS STABILIZATION WITH THE CONDITION NUMBER

1. Singularity Problem

As discussed in the simulation result section, singularity problem frequently occurs when the number of shots for VQS is low. Figure 8 shows a typical example of the simulation with and without singularity. Graph (a) illustrates the VQS without singularity. Although the

rate function fluctuates around the correct value, there is no sudden deviation. On the contrary, the rate function abruptly deviates from the correct value, and the fidelity between simulated state and the exact state suddenly drops from one in the plot (c). Both simulations (a) and (c) started from the same initial state.

It is deduced that singularity occurs when the matrix M in Eq. 16 approaches a singular matrix. The original differential Eq. 16 is as follows:

$$\sum_j M_{i,j} \frac{d\lambda_j}{dt} = V_i. \tag{16}$$

The matrix M for the ansatz in Figure 1 is a 10×10 matrix. When $M_{i,j}$ is ill-conditioned, a small perturbation to matrix elements $M_{i,j}$ and vector elements V_i results in a substantial fluctuation in the ansatz parameter λ_j. Due to the probabilistic nature of the measurement process for each entry, the occurrence of singularity-related issues is possible at any given time. This hypothesis is verified by calculating the *condition number*.

2. Definition of the Condition Number

Throughout this paper, the Euclidean norm is used for a vector space $\mathbb{C}^n$, defined as $\|x\| = \sqrt{\sum_i |x_i^2|}$. The subordinate matrix norm on $\mathbb{C}^{n\times n}$ is then defined as

$$\|A\| := \max_{x\neq 0} \frac{\|Ax\|}{\|x\|} = \text{the largest singular value of } A. \tag{A1}$$

The purpose of defining the condition number is to measure the effect of perturbation to A and b when solving the linear equation $Ax = b$, where $A \in \mathbb{C}^{n\times n}$, and $x,\ b \in \mathbb{C}^n$. The matrix condition number of a nonsingular matrix $A \in \mathbb{C}^{n\times n}$ is defined by [4]

$$\begin{aligned}\kappa(A) &:= \lim_{\epsilon\to 0} \sup_{\|\Delta A\| \le \epsilon \|A\|} \left(\frac{\left\| (A+\Delta A)^{-1} - A^{-1} \right\|}{\epsilon \left\| A^{-1} \right\|} \right) \\ &= \|A\| \left\| A^{-1} \right\|. \end{aligned} \tag{A2}$$

Let $E \in \mathbb{C}^{n\times n}$ be an arbitrary matrix and $f \in \mathbb{C}^n$ be an arbitrary vector. Then, the *normwise condition number* is defined by

$$\kappa_{E,f}(A,x) := \lim_{\epsilon\to 0} \sup \left\{ \frac{\|\Delta x\|}{\epsilon \|x\|} \middle| (A+\Delta A)(x+\Delta x) = b + \Delta b, \right.$$
$$\left. \|\Delta A\| \le \epsilon \|E\|, \quad \|\Delta b\| \le \epsilon \|f\| \right\}. \tag{A3}$$

When $E = A$ and $f = b$, we have [4]

$$\kappa(A) \le \kappa_{E,f}(A,x) \le 2\kappa(A). \tag{A4}$$

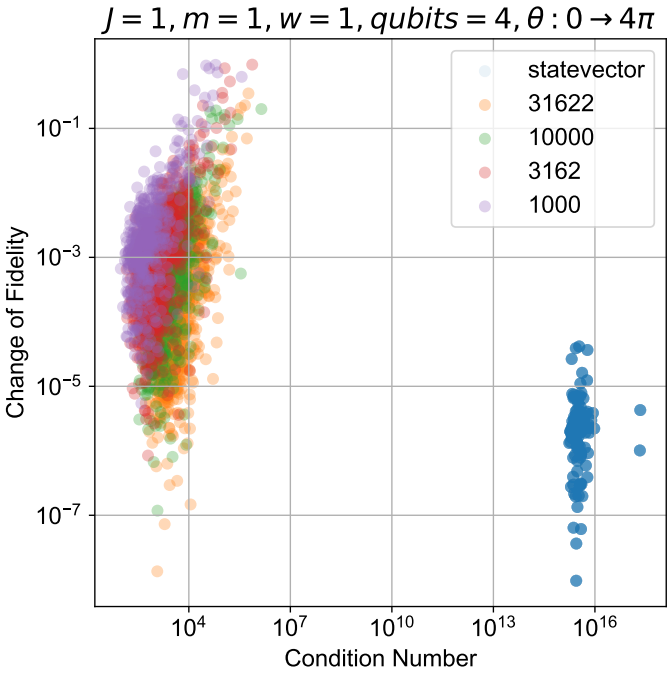

FIG. 9. Condition number versus the change of fidelity. For each number of shots (varied from 1000 to 31622) and statevector simulation, simulation was repeated 15 times from the same initial state. A simulation is stopped if its fidelity changes more than 0.1 or after 100 iterations. There are 451 points for 1000 shots, 930 points for 3162 shots, 966 points for 10000 shots, 1299 points for 31622 shots, and 1500 points for statevector.

Therefore, the condition number gives the maximum sensitivity of the solution to the equation $Ax = b$ concerning perturbations applied to A and b.

Figure 8 (b)/(d) is the condition number of the VQS simulation (a)/(c). Red vertical marker is drawn at the singularity point of graph (d). It is remarkable that the condition number is particularly large at that point.

To evaluate the relationship between the condition number and the error of VQS more quantitatively, the condition number and the fidelity change is plotted on Figure 9. The figure indicates that the condition number increases as the number of shots increases, and generally shifting toward the statevector simulation results, where the condition number is high and the fidelity change is low.

Figure 10 shows the probability density function of the distribution of the condition number and the fidelity change. For simulation with shots, fidelity is more likely to fluctuate as the condition number increases. However, such correlation is not confirmed for the statevector simulation. Moreover, the overall distribution has larger condition number and lower change of fidelity as the number of shots increases. The shape of the graph for each number of shots indicates that sudden change of fidelity occurs due to an ill-conditioned matrix.

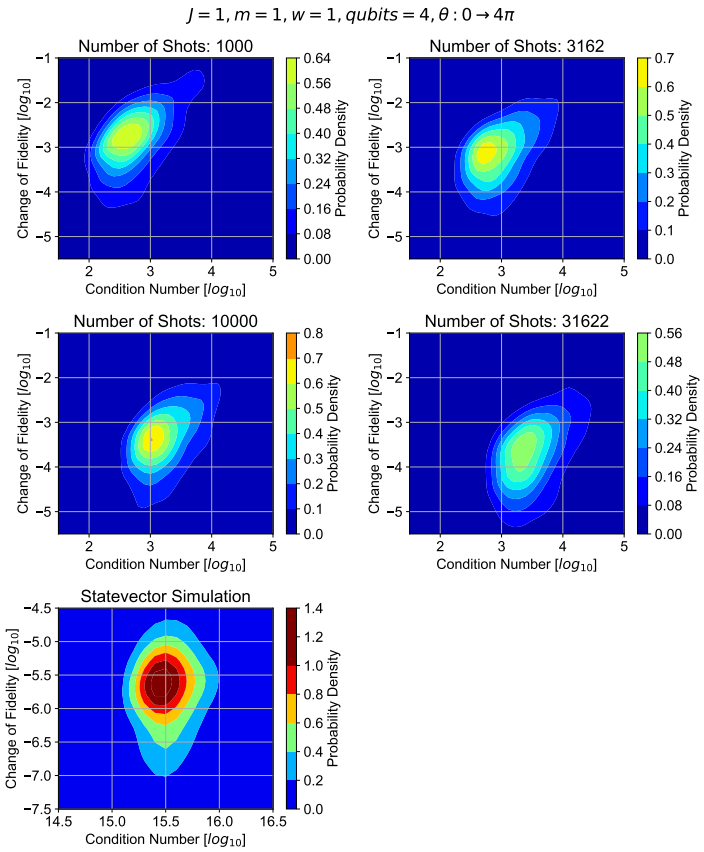

FIG. 10. Probability density function calculated with the Gaussian kernel density estimation. Scott's rule is used for the kernel density estimation [3]. Using data plotted on Figure 9.

These observations suggest the following algorithm to avoid the singularity problem.

1. Set threshold of the condition number.

2. During the simulation of the VQS, calculate the condition number every time.

3. If the condition number exceeds the threshold, calculate that step again until the condition number becomes lower than the threshold.

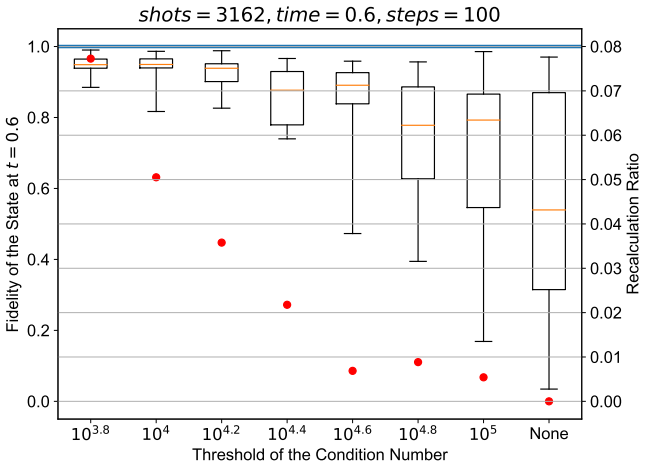

FIG. 11. Fidelity and the recalculation probability of the condition number algorithm. Recalculation probability is the probability that the condition number exceeds the threshold. $J = 1, m = 1, w = 1, \theta : 0 \to 4\pi$. There are 20 trials for each threshold. No threshold means VQS continues no matter how large the condition number is. Box plots shows the fidelity between the accurate state and the simulated state at $t \cdot g = 1.2$ (left). Red points show the recalculation ratios (right).

Figure 11 shows the result of the algorithm. The threshold of the recalculation ranges from $10^{3.8}$ to 10^{5}. The figure illustrates that lower threshold keeps the right trajectory of the simulation. This figure signifies the efficienty of the condition number algorithm.

Appendix B: DOWNLOADING THE SAMPLE CODE

Please refer to https://github.com/ShintaroAe/VQE-VQS-simulation-Schwinger-Model for the source code of this project. VQE and VQS is implemented on `topological_dynamics.py`. The simulation is also implemented using the exact diagonalization in `topological_dynamics.py`. `11_15_example.ipynb` is the instruction of these codes. `LE_params_statevector_steps_3000_J1_m1_w1_numqubits4_theta0_deltheta4pi_duration6_initfid0_999801.npy` is a parameter example of the time evolution. These files can be downloaded and run on your remote environement.

[1] Minimize(method='COBYLA') — SciPy v1.11.4 Manual. https://docs.scipy.org/doc/scipy/reference/optimize.minimize-cobyla.html.

[2] A. Casher, J. Kogut, and Leonard Susskind. Vacuum polarization and the absence of free quarks. *Physical Review D*, Vol. 10, No. 2, pp. 732–745, July 1974.

[3] David W. Scott. *Multivariate Density Estimation: Theory, Practice, and Visualization*. John Wiley & Sons, Inc., March 2015.

[4] Nicholas J. Higham. *Accuracy and Stability of Numerical Algorithms*. Society for Industrial and Applied Mathematics, 2 edition, 2002.

[5] Masazumi Honda, Etsuko Itou, Yuta Kikuchi, Lento Nagano, and Takuya Okuda. Classically emulated digi-

tal quantum simulation for screening and confinement in the Schwinger model with a topological term. *Physical Review D*, Vol. 105, No. 1, p. 014504, January 2022.

[6] Michael A. Nielsen and Isaac L. Chuang. *Quantum Computation and Quantum Information: 10th Anniversary Edition*. Cambridge University Press, December 2010.

[7] Kosuke Mitarai and Keisuke Fujii. Methodology for replacing indirect measurements with direct measurements. *Physical Review Research*, Vol. 1, No. 1, p. 013006, August 2019.

[8] Niklas Mueller, Joseph A. Carolan, Andrew Connelly, Zohreh Davoudi, Eugene F. Dumitrescu, and Kübra Yeter-Aydeniz. Quantum computation of dynamical quantum phase transitions and entanglement tomography in a lattice gauge theory, October 2022.

[9] Lento Nagano, Aniruddha Bapat, and Christian W. Bauer. Quench dynamics of the Schwinger model via variational quantum algorithms. *Physical Review D*, Vol. 108, No. 3, p. 034501, August 2023.

[10] Alberto Peruzzo, Jarrod McClean, Peter Shadbolt, Man-Hong Yung, Xiao-Qi Zhou, Peter J. Love, Alán Aspuru-Guzik, and Jeremy L. O'Brien. A variational eigenvalue solver on a photonic quantum processor. *Nature Communications*, Vol. 5, No. 1, p. 4213, July 2014.

[11] Roeland Wiersema, Cunlu Zhou, Yvette de Sereville, Juan Felipe Carrasquilla, Yong Baek Kim, and Henry Yuen. Exploring entanglement and optimization within the Hamiltonian Variational Ansatz. *PRX Quantum*, Vol. 1, No. 2, p. 020319, December 2020.

[12] Xiao Yuan, Suguru Endo, Qi Zhao, Ying Li, and Simon Benjamin. Theory of variational quantum simulation. *Quantum*, Vol. 3, p. 191, October 2019.

[13] T. V. Zache, N. Mueller, J. T. Schneider, F. Jendrzejewski, J. Berges, and P. Hauke. Dynamical topological transitions in the massive Schwinger model with a {\theta}-term. *Physical Review Letters*, Vol. 122, No. 5, p. 050403, February 2019.